Photoelectron diffraction of the Si(111)-$(\sqrt{3}\times\sqrt{3})R30°$-Ga surface: Local atomic structure and vibrational correlation

T. Hanada*
Department of Physics, Graduate School of Science, University of Tokyo, Tokyo 113, Japan

H. Daimon
Department of Physics, Graduate School of Science, University of Tokyo, Tokyo 113, Japan
and Department of Material Physics, Faculty of Engineering Science, Osaka University, Toyonaka 560, Japan

S. Nagano and S. Ino
Department of Physics, Graduate School of Science, University of Tokyo, Tokyo 113, Japan

S. Suga
Department of Material Physics, Faculty of Engineering Science, Osaka University, Toyonaka 560, Japan

Y. Murata
Division of Natural Science, The University of Electro-Communications, Chofu 182, Japan
(Received 18 November 1996)

The kinetic-energy dependence of the polar-angle photoelectron diffraction of Ga $3d$ emission was measured on the Si(111)-$(\sqrt{3}\times\sqrt{3})R30°$-Ga surface using synchrotron radiation. The energy-dependent variations in the polar-angle intensity distribution can be reproduced by model calculations essentially assuming one scattering Si atom 2.6 Å below the Ga photoelectron emitter. This fact clearly indicates that the Ga atom adsorbs at the site directly above a second-layer Si atom (T_4 site). Calculations of the photoelectron diffraction using larger clusters have revealed that the vibrational correlation between the Ga adatom and the Si atom directly below it is very strong. This correlation effect emphasize the scatterings by the Si atom directly below the emitter compared with those by other surrounding atoms. [S0163-1829(97)07524-3]

I. INTRODUCTION

Surface equilibrium and dynamical structures have been investigated using various methods. Photoelectron diffraction is suitable for the analysis of local surface structure, particularly surrounding the adsorbate.[1,2] This method usually analyzes the energy or the angular dependence of core-level-photoelectron intensities modified by the scatterings by surrounding atoms. The x-ray photoelectron diffraction (XPD) using high-energy radiations such as Mg $K\alpha$ or Al $K\alpha$ mainly measures forward-focusing peaks which indicate the directions of the scattering atoms. An azimuthal scan of XPD at low takeoff angles is sensitive to the in-plane surface structure.[3] As far as photoelectrons emitted from an uppermost layer are concerned, however, the forward scatterings detectable outside the crystal take place only at nearly zero takeoff angles, and contain little information about the structure of the underlying layers. Using low-energy soft-x-ray radiation, backscatterings by the substrate become strong enough at positive takeoff angles to provide information about the substrate structure. At this energy range, polar-angle photoelectron diffraction (PPD) is appropriate for the analysis of the structure parameters in the surface-normal direction because the vertical component of momentum transfer of photoelectron is varied by the scan.[4]

In the previous paper, the analysis of the kinetic-energy dependence of the PPD from the Si(111)-$(\sqrt{3}\times\sqrt{3})R30°$-Al surface has revealed that an Al atom is located at 2.57 Å directly above a Si atom.[5] This indicates that Al adsorbs at the fourfold-coordinated top site (T_4) (Refs. 5–12) because the distance is consistent with that between an Al adatom and second-layer Si and there is no such surface-normal interatomic distance in the threefold-coordinated hollow site (H_3) model (Fig. 1).

In the present work, we applied this method to analyze the local structure of the Si(111)-$(\sqrt{3}\times\sqrt{3})R30°$-Ga surface. By comparing Al $2p$ and Ga $3d$ photoelectron diffraction patterns, it was found that anisotropy which depends on the

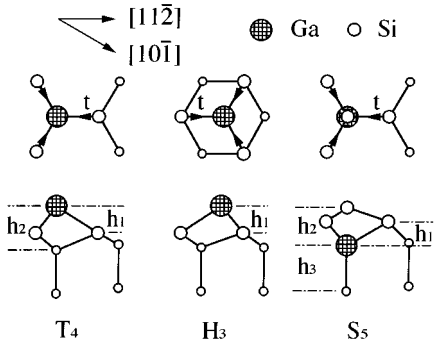

FIG. 1. Top and side views of the T_4, H_3, and S_5 models for the Si(111)-$(\sqrt{3}\times\sqrt{3})R30°$-Ga surface. The structure parameters of the first neighbors of the Ga atom, h_1, h_2, h_3, and t, used for the optimization are illustrated.

parity of the photoelectron wave function is a crucial factor. Roughly speaking, at the same kinetic energy of the photoelectrons, a broad intensity maximum (minimum) in the Ga $3d$ PPD pattern turns to a minimum (maximum) in the Al $2p$ PPD pattern. Since the difference in the geometric structure is small between the two surfaces, this reversal of features between the two PPD patterns can be attributed to the difference in the parity of the photoelectron which depends on the initial-state symmetry (d or p).

We also found that vibrational correlation is important for the quantitative analysis of the photoelectron diffraction of this surface. The backscatterings by the atoms which vibrate in phase with the emitter are highly emphasized compared with those by the other atoms because the Debye-Waller-like factor of photoelectron diffraction is a function of mean-square thermal displacement of a scatterer relative to the emitter. Owing to the distinctive structure of the T_4 model the Ga adatom and the atom directly below it are strongly correlated.

II. EXPERIMENT

Measurements were performed at the third beamline of SOR-RING (0.4-GeV electron storage ring) of the Institute for Solid State Physics, the University of Tokyo. This beamline utilizes linearly polarized light from a bending magnet. The apparatus for the angle-resolved photoemission spectroscopy contains a hemispherical electron energy analyzer mounted on a turntable and a plane grating UHV monochromator which has been described elsewhere.[13] The residual gas pressure was 8×10^{-9} Pa.

A mirror-polished (111) surface of p-type silicon wafer with a resistivity of 20 Ω cm was used. To obtain a clean surface, the specimen was heated to 1500 K by an electric current passing directly through it. Ga was deposited from W filament onto the clean Si(111) surface showing the 7×7 structure at the substrate temperature of 810 K. At this temperature, the reflection high-energy electron-diffraction (RHEED) pattern completely changes from 7×7 to $\sqrt{3}\times\sqrt{3}$ at $\frac{1}{3}$ monolayer coverage. The deposition was stopped when the sharp and pure $\sqrt{3}\times\sqrt{3}$ pattern was obtained.

The angle between the incident direction of the light and surface-normal direction was set to be 60° as shown in Fig. 2. The electric vector of the light was in the incident plane (p polarized). Intensities of the Ga $3d$ photoelectrons normalized by photon flux were measured as a function of the polar angle θ, keeping the sample fixed and rotating the electron analyzer in the incident plane. The binding energy of the Ga $3d$ core level was 18.5 eV. The PPD patterns were measured at $[11\bar{2}]$ and $[10\bar{1}]$ incident azimuths and at four kinetic energies (in vacuum) of the Ga $3d$ photoelectron, i.e., 140, 160, 180, and 200 eV.

III. EXPERIMENTAL RESULTS AND INTERPRETATION

Obtained PPD patterns are shown by dots in Fig. 3. Disregarding diffraction effects, the curves are expected to show maxima around $\theta=30°$ because photoelectrons are ejected around the electric vector of the incident light as shown in Fig. 2(a). The attenuation of the photoelectrons by inelastic

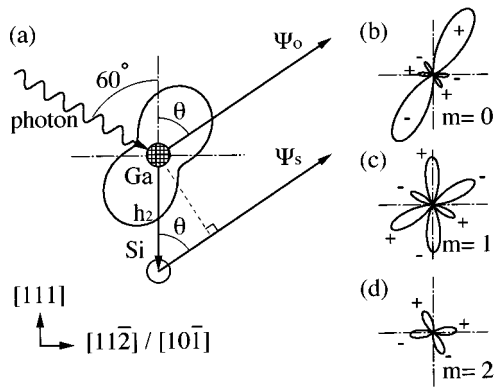

FIG. 2. Schematic diagram of PPD. Interference occurs between the direct wave Ψ_0 from an emitter Ga atom and the wave Ψ_s scattered by the surrounding atoms. θ is the polar angle of the detector. In the present experiment, the incident angle of the p polarized photon is 60°. The intensity distribution of direct Ga $3d$ photoelectron at kinetic energy of 200 eV is shown around the Ga atom (a). The intensity and sign distributions of magnetic quantum number $m=0$ (b), 1 (c), and 2 (d) components of the direct wave are also shown. Intensities of $m=-1$ and -2 components are zero on the incident plane.

scatterings decreases the intensity still more at higher polar angles. Diffraction effects make the angular distribution more complex. It is most appealing that the broad peaks and dips around the arrows in Fig. 3 move with the kinetic energy. In contrast, the azimuthal dependence is small. This means that the scatterers along the surface-normal direction contribute to the diffraction patterns more than those not lying along surface normal.

The broad peaks and dips in Fig. 3 can be assigned to a specific interference between the direct wave and a scattered

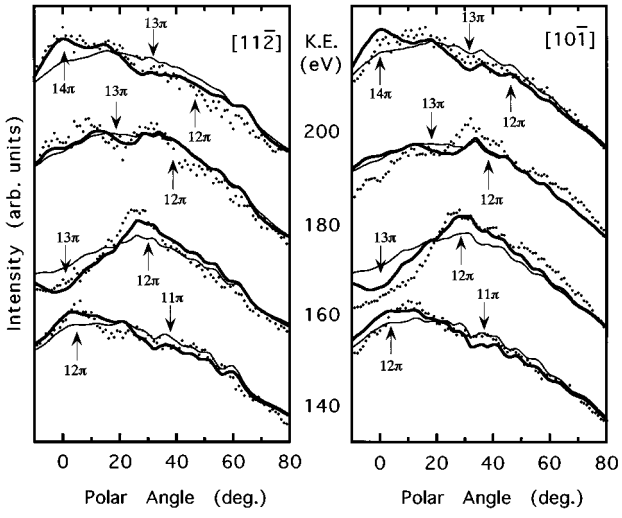

FIG. 3. Experimental PPD patterns for the $[11\bar{2}]$ and $[10\bar{1}]$ azimuth are plotted by dots. Calculated patterns for the optimal and uncorrelated T_4 models are plotted by thick and thin lines, respectively. Kinetic energies of the Ga $3d$ core photoelectrons are indicated in the center. Upward and downward arrows indicate peaks and dips, respectively, expected from the phase difference between the direct wave and the wave scattered by Si which is 2.58 Å directly below the Ga.

wave by path-length-difference consideration similarly to the Al adsorbed surface.[5] The T_4 model has a second-layer Si atom directly below the Ga adatom as shown in Fig. 1. Here, we show that the existence of this Si atom is consistent with the PPD results, and that the T_4 model provides better agreement than the H_3 model. Figure 2(a) shows this situation schematically. Interference occurs between the direct wave Ψ_0 and the wave Ψ_s scattered by the Si atom directly below the emitter. The phase difference Δ between Ψ_0 and Ψ_s is given by

$$\Delta = \pi + kh_2(1+\cos\theta) + \delta, \tag{1}$$

where k is the wave number of the photoelectron, δ is the phase shift due to the scattering by the Si atom, θ is the polar angle of the detected wave, and h_2 is the distance between the Ga adatom and the Si atom.

The first term π in the right-hand side of Eq. (1) is because the parity of the Ga $3d$ photoelectron (having p and f symmetry) is odd and the detector and the scatterer are located at opposite directions. Generally speaking, from the selection rule of the dipole transition, the magnetic quantum number m of the initial state is preserved; for each m, there are two allowed channels from initial angular momentum l to final $l-1$ and $l+1$. In Figs. 2(b)–2(d), intensity distribution of the direct Ga $3d$ photoelectron for each initial m component is shown according to Ref. 14. In addition, the sign of the photoelectron wave function is indicated considering only the $f(l+1)$ channel because this channel is dominant in the concerning energy range.[14] As shown in Figs. 2(b)–2(d), the phase of the wave emitted toward the scatterer is opposite to that emitted directly toward the detector at θ up to about 30°.

When Δ is the even (odd) multiple of π, the intensity shows maximum (minimum). The upward and downward arrows in Fig. 3 indicate the polar angles at which the direct and the scattered waves are in phase and out of phase, respectively, assuming $h_2 = 2.58$ Å. The mean inner potential of Si was set to be 12 eV to evaluate k in the sample and the refraction at the vacuum-sample interface. The phase shift δ due to the scattering is a slowly varying function of kinetic energy and scattering angle $\pi-\theta$ in the backscattering region. In this estimation it was set to be 2.0 rad, the mean value for the scatterings by the Si atom at a scattering angle ranging from 120–180° and at a kinetic energy of 140 and 200 eV.

As shown in Fig. 3, with increasing kinetic energy, the peaks (dips) due to the same phase difference Δ move toward higher polar angles. The predicted angles of the peaks (upward arrow) and dips (downward arrow) assuming $h_2 = 2.58$ Å are in good agreement with the experimental results. For example, at kinetic energy $E_k = 160$ eV, the PPD patterns have a dip at normal direction and have a peak at $\theta = 30°$. The value $h_2 = 2.58$ Å is very close to the sum of the covalent radii of Ga and Si. Therefore, the T_4 model is more appropriate than H_3 model because the T_4 model has an Si atom just below the Ga atom while the H_3 model does not. From Eq. (1), the 3-eV error in the estimation of the mean inner potential causes about a 0.02-Å error of h_2. Therefore, this geometrical parameter is only little affected by the assumed value of the mean inner potential.

IV. INTENSITY CALCULATIONS

Next, we calculated intensities to confirm the above estimation quantitatively. The calculation method is a single scattering cluster theory[1,2,4] extended to include the anisotropy of the direct wave,[14] the spherical wave correction for emission and scattering,[5] and double scattering. Consequently, the photoelectron wave function consists of a series expansion up to the second-order term $\Psi_0+\Psi_1+\Psi_2$ of Ref. 15. Additionally, the thermal average[16] is incorporated as follows.

Owing to the thermal vibration, diffraction intensities must be averaged over various instantaneous arrangements of the atoms. Since the photoemission and scattering process take place much faster than the atomic vibration, the photoelectron is scattered by the atom at $(\mathbf{r}_s+\mathbf{u}_s)-(\mathbf{r}_0+\mathbf{u}_0) = (\mathbf{r}_s-\mathbf{r}_0)+(\mathbf{u}_s-\mathbf{u}_0)$ at each emission event, where $\mathbf{r}_0$ and $\mathbf{r}_s$ are equilibrium position vectors of the emitter and the scatterer and $\mathbf{u}_0$ and $\mathbf{u}_s$ are thermal displacement vectors of them, respectively. The thermal average can be approximately carried out by using the atomic scattering factor multiplied by the square-root of the Debye-Waller-like factor $\exp(-W/2)$, where $W=\langle(\Delta\mathbf{k}\cdot\Delta\mathbf{u}_s)^2\rangle$, the mean-square of the inner product of the momentum transfer $\Delta\mathbf{k}$ and the relative displacement vector $\Delta\mathbf{u}_s=\mathbf{u}_s-\mathbf{u}_0$. It is convenient to use the projection of the displacements onto the momentum transfer $\Delta\mathbf{k}$; $W=\Delta k^2\langle\Delta u_{sp}^2\rangle$ and $\langle\Delta u_{sp}^2\rangle=\langle(u_{sp}-u_{0p})^2\rangle = \langle u_{sp}^2\rangle+\langle u_{0p}^2\rangle-2\langle u_{sp}u_{0p}\rangle$, where the subscript p denotes the projection.

If the thermal motion of the two atoms are uncorrelated, correlation function $\langle u_{sp}u_{0p}\rangle=0$ and $W=\Delta k^2(\langle u_{sp}^2\rangle + \langle u_{0p}^2\rangle)$. It is the case with a distant pair of atoms. As for conventional diffraction experiments using the incident beam spread over the sample, vibrational correlations have little contribution because most of the atomic pairs which are picked up arbitrarily are distant ones. In contrast, since the photoelectrons are scattered most strongly by nearest neighbors, vibrational correlation cannot be ignored. The vibrational amplitude is inversely proportional to the frequency. Consequently, low-frequency acoustic-phonon modes have the largest contribution to the root-mean-square projection of displacements (RMSPD's) $\langle u_{sp}^2\rangle^{1/2}$ and $\langle u_{0p}^2\rangle^{1/2}$. In this mode, however, neighboring atoms move almost in phase and the correlation function is positive. Therefore, the root-mean-square projection of the relative displacement RMSPRD $\langle\Delta u_{sp}^2\rangle^{1/2}$ of neighboring atoms would be significantly smaller than the uncorrelated one because the largest contribution in $\langle u_{sp}^2\rangle$ and $\langle u_{0p}^2\rangle$ is canceled out by $\langle u_{sp}u_{0p}\rangle$. In fact, RMSPRD of the nearest neighbors has been calculated to be about half of that of the uncorrelated pair for bulk Si crystal at room temperature.[17]

The RMSPD's of Ga adatom and Si bulk atom have been measured experimentally to be about 0.1 Å (Ref. 18) and 0.07 Å, respectively, at room temperature. Therefore, at first, the RMSPRD of the nearest neighbor of the emitter was set to be 0.06 Å considering the correlation. The RMSPRD's of other atoms were approximated to be that of uncorrelated values, that is 0.14 Å for Ga and 0.12 Å for Si. In the present analysis, the thermal displacements were assumed to be isotropic. The mean inner potential and inelastic attenuation length were set to be 12 eV and 10 Å, respectively.

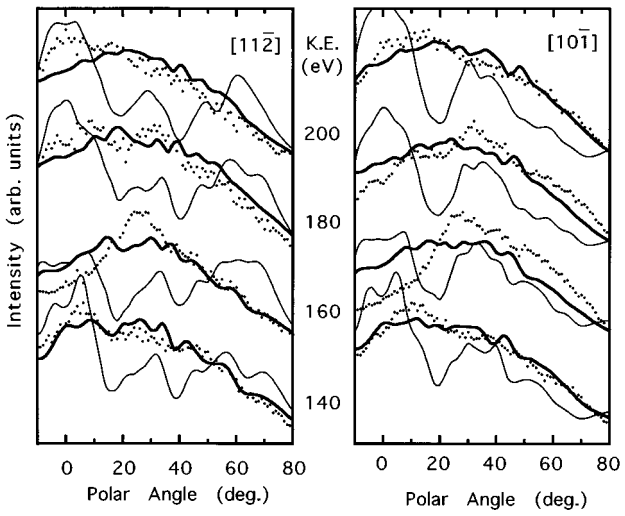

FIG. 4. Experimental PPD patterns for the [11$\bar{2}$] and [10$\bar{1}$] azimuths are plotted by dots. Calculated patterns for the H_3 and S_5 models are plotted by thick and thin lines, respectively. Kinetic energies of the Ga 3d core photoelectrons are indicated in the center.

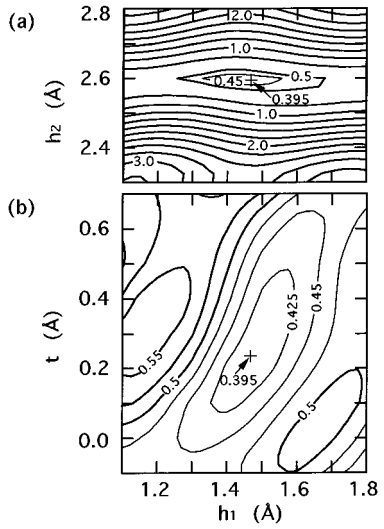

FIG. 5. (a) R-factor contour plot for the T_4 model as a function of h_1 and h_2, where $t=0.23$ Å. (b) R-factor contour plot for the T_4 model as a function of h_1 and t, where $h_2=2.60$ Å. Structure parameters are illustrated in Fig. 1.

Calculations were made using clusters consisting of about 100 atoms for the three models in Fig. 1. As shown in Fig. 1, structure parameters of the nearest-neighbor Si atoms are moved choosing the T_4, H_3, and S_5 (Ref. 19) models. Here, t is surface-parallel displacement from the unreconstructed position of the first-layer atom and h_1, h_2, and h_3 are surface-normal distances between the adatom and the nearest-neighbor atoms. Other coordinates about the substrate Si atoms are determined by the minimization of the Keating's strain energy[20] fixing the positions of the nearest neighbors and their symmetry equivalent atoms because scatterings from the atoms other than the nearest neighbors are weak as described later. The R factor R_{PPD} used to quantify the agreement between the calculations and the experiment is identical to R of Ref. 12, except that R_{PPD} is normalized to R of the unscattered intensity, i.e., R_{PPD} becomes unity for the isolated emitter model having no diffraction effect.

The calculated PPD patterns for the optimized H_3 and S_5 models are shown in Fig. 4 by thick and thin lines, respectively. Obviously, the calculated curves for S_5 model are not consistent with experiment owing to strong forward-focusing peaks at 0° by the Si adatom and at 60° of [112] incidence by the first-layer Si atom. The peaks at 30° are due to interference of the direct wave and the wave scattered by the Si adatom. These strong peaks do not move with the kinetic energy. Similarly, models in which Ga is embedded below Si atoms are easily ruled out. The calculated curves for H_3 model also show only a little dependence on the kinetic energy even if the structure parameters are moved in wide range. The minimum R factors for the S_5 and H_3 models are 6.2 and 0.9, respectively.

The calculated PPD patterns for the optimal T_4 model are shown in Fig. 3 by thick lines. Agreement of the T_4 model with experiment is obviously better than that of the other models. At the final stage, the R factor was minimized not only for the three structure parameters indicated in Fig. 1 but for RMSPRD's, mean inner potential, and inelastic attenuation length by using the simplex method.[21] The structure parameters of the optimal T_4 model were $h_2=2.60$, $h_1=1.46$, and $t=0.23$ Å. The RMSPRD of the Si directly below the Ga emitter, the nearest-neighbor Si in first layer, other Si, and other Ga were 0.02, 0.09, 0.3, and 0.2 Å, respectively. The mean inner potential was 10.5 eV and the inelastic attenuation length was 11.6 Å. R factor for the optimal T_4 structure was $R_{\mathrm{PPD}}=0.39$, where R in the form of Ref. 12 is 0.01. Figure 5 shows R-factor contour maps; the parameters other than those of two axes are fixed at the optimal values. The R factor for the T_4 model shows a deep minimum about the parameter h_2. In contrast, coordinates of the first-layer atom cannot be determined with enough accuracy.

V. DISCUSSION

All prominent structures in the PPD patterns appear at the polar angle lower than 30°. In this range, the photoelectrons are backscattered by the Si atom directly below the emitter at the scattering angle larger than 150° and the momentum transfer is almost normal to the surface. Therefore, the PPD patterns are sensitive to the surface-normal components of the position and the thermal displacement of the scatterer. Figure 6 shows the R factor of the optimized T_4 structure as a function of the RMSPRD's. From this figure, RMSPRD of the nearest-neighbor Si in second layer, $\langle \Delta u_2^2 \rangle^{1/2}$, is considered to be smaller than 0.06 Å, i.e., half of the uncorrelated value. If the uncorrelated value $\langle \Delta u_2^2 \rangle^{1/2}=0.12$ Å is used, the PPD patterns for the same T_4 structure become thin lines in Fig. 3, whose R factor is 0.7. The RMSPRD's of the second neighbors and further Si atoms are considered to be larger than 0.15 Å, which is thought to be uncorrelated.

In Fig. 7, Debye-Waller-like factor $\exp\{2k^2(\cos\alpha-1)\langle \Delta u_{sp}^2 \rangle\}$ for the 150-eV electron is plotted as a function of

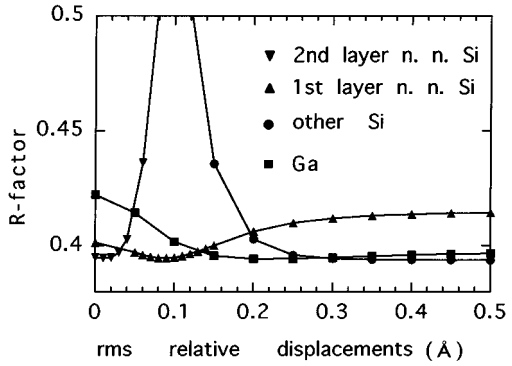

FIG. 6. R factor for the optimal geometric structure of the T_4 model as a function of root-mean-square (rms) projection of relative displacements (RMSPRD's) of the nearest-neighbor Si atoms in the second and first layers, other Si atoms, and Ga atoms other than the emitter.

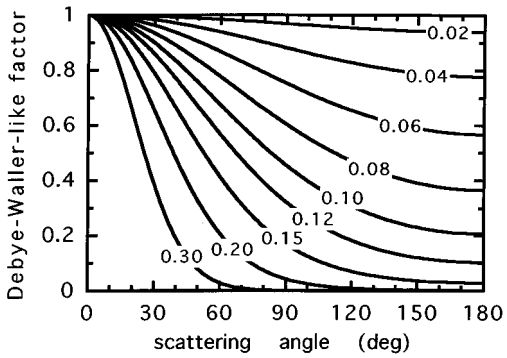

FIG. 7. Debye-Waller-like factor as a function of scattering angle for 150-eV electron at various isotropic root-mean-square projection of relative displacements (RMSPRD's) (in Å) indicated in the figure.

scattering angle α, at various isotropic RMSPRD's. Figure 7 indicates that the correlation effect relatively emphasizes the backscatterings from the atom directly bellow the emitter and that effective scatterings from the atoms other than the nearest neighbors are very weak because of the strong cancellation due to the thermal average with RMSPRD's larger than 0.15 Å. As a result, peaks and dips appear in the PPD patterns as shown by the arrows in Fig. 3 following the simple prediction with Eq. (1). Figure 7 also shows that diffraction intensity is sensitive to the RMSPRD under the backscattering condition. When the RMSPRD exceeds 0.2 Å, however, effective backscatterings vanish and the estimation of the RMSPRD becomes difficult.

In the T_4 model, adatom, second- and third-layer atoms align in surface-normal direction, so potential barriers for their motion against each other are likely to be steep. Consequently, their thermal motions are highly correlated to keep their interatomic distances nearly constant. A very high-frequency phonon mode assigned to the stretching of these bonds has been observed around 65 meV on the Si(111)-$(\sqrt{3}\times\sqrt{3})R30°$-Ga surface using high-resolution electron energy-loss spectroscopy.[22] The mode is characteristic of the Si(111) surface having T_4 adatoms.[23,24]

As far as high-energy photoelectron is concerned, forwardscattering is dominant, and only the wave emitted toward the scatterer contributes to the intensity. Therefore, the parity of the photoelectron wave function has no influence upon the intensity distribution. In contrast, it has a critical importance for the analysis of low-energy photoelectron, which is backscattered strongly. Comparison between the Ga $3d$ and the Al $2p$ (Ref. 5) PPD patterns from the $\sqrt{3}\times\sqrt{3}$ surfaces clearly demonstrates the importance. These two surfaces have the same topological structure and atomic coordinates are also very similar. The PPD patterns of the two surfaces at the same kinetic energy of photoelectrons are, however, very different. This is because the parities of the Ga $3d$ and Al $2p$ photoelectron wave functions are odd and even, respectively. Therefore, the first term in the right-hand side of Eq. (1) is zero for Al $2p$ and a broad peak (dip) in the Ga $3d$ pattern turns into a dip (peak) of the Al $2p$ pattern at the same kinetic energy.

Finally, experimental results of the present study are in good agreement with double-scattering calculations. Presumably, the reduction of the spherical wave amplitude being inversely proportional to distance, attenuation by the inelastic scattering, and the vibrational correlation effects would cooperate to restrict the region in which strong scatterings take place into the cluster of nearest-neighbor scatterers. As a result, higher-order multiple scatterings by a series of atoms would be negligible though the interaction of low-energy electron with the atom is large.

VI. CONCLUSION

Polar-angle photoelectron diffraction was successfully applied to the Si(111)-$(\sqrt{3}\times\sqrt{3})R30°$-Ga surface structure analysis. It was found that there is a Si atom located at 2.60 Å directly below the Ga atom. This fact indicates that the adsorption site of the Ga atom is the T_4 site. The interatomic distance was determined accurately from the energy-dependent variations of the PPD pattern. The anisotropic emission distribution of the unscattered photoelectron and the vibrational correlation between neighboring atoms must be included appropriately in the calculation of low-energy photoelectron diffraction. Thermal displacements of the Ga adatom and the Si atom directly below it are strongly correlated.

ACKNOWLEDGMENTS

The authors are grateful to the staff of Synchrotron Radiation Laboratory, the Institute for Solid State Physics, the University of Tokyo. Dr. K. Terakura is gratefully acknowledged for the computation program of the partial-wave phase shifts.

*Present address: Institute for Materials Research, Tohoku University, Sendai 980-77, Japan.
[1] C. S. Fadley, in *Synchrotron Radiation Research: Advances in Surface Science*, edited by R. Z. Bachrach (Plenum, New York, 1990).
[2] S. A. Chambers, Adv. Phys. **40**, 357 (1991).
[3] K. Higashiyama, S. Kono, and T. Sagawa, Surf. Sci. **175**, L794 (1986).
[4] H. Daimon, H. Ito, S. Shin, and Y. Murata, J. Phys. Soc. Jpn. **53**, 3488 (1984).
[5] H. Daimon, S. Nagano, T. Hanada, S. Ino, S. Suga, and Y. Murata, Surf. Sci. **221**, 244 (1989).
[6] J. E. Northrup, Phys. Rev. Lett. **53**, 683 (1984).
[7] A. Kawazu and H. Sakama, Phys. Rev. B **37**, 2704 (1988).
[8] J. Nogami, S. Park, and C. F. Quate, Surf. Sci. **203**, L631 (1988).
[9] J. Zegenhagen, J. R. Patel, P. Freeland, D. M. Chen, J. A. Golovchenko, P. Bedrossian, and J. E. Northrup, Phys. Rev. B **39**, 1298 (1989).
[10] H. Huang, S. Y. Tong, W. S. Yang, H. D. Shih, and F. Jona, Phys. Rev. B **42**, 7483 (1990).
[11] H. Wu, G. J. Lapeyre, H. Huang, and S. Y. Tong, Phys. Rev. Lett. **71**, 251 (1993).
[12] T. Hanada, H. Daimon, and S. Ino, Phys. Rev. B **51**, 13 320 (1995).
[13] S. Suga, M. Taniguchi, S. Shin, H. Sakamoto, M. Yamamoto, M. Seki, Y. Murata, and H. Daimon, Nucl. Instrum. Methods **222**, 80 (1984).
[14] S. M. Goldberg, C. S. Fadley, and S. Kono, J. Electron Spectrosc. Relat. Phenom. **21**, 285 (1981).
[15] M. Biagini, Phys. Rev. B **48**, 2974 (1993).
[16] J. J. Barton, S. W. Robey, and D. A. Shirley, Phys. Rev. B **34**, 778 (1986).
[17] H. Sandfort, A. Mazur, and J. Pollmann, Phys. Rev. B **51**, 7168 (1995).
[18] R. E. Martinez, E. Fontes, J. A. Golovchenko, and J. R. Patel, Phys. Rev. Lett. **69**, 1061 (1992).
[19] I.-W. Lyo, E. Kaxiras, and Ph. Avouris, Phys. Rev. Lett. **62**, 1261 (1989).
[20] P. N. Keating, Phys. Rev. **145**, 637 (1966).
[21] J. A. Nelder and R. Mead, Comput. J. **7**, 308 (1965).
[22] J. Schmidt, H. Ibach, and J. E. Müller, Phys. Rev. B **51**, 5233 (1995).
[23] W. Daum, H. Ibach, and J. E. Müller, Phys. Rev. Lett. **59**, 1593 (1987).
[24] P. Akavoor, G. S. Glander, L. L. Kesmodel, and K. Burke, Phys. Rev. B **48**, 12 063 (1993).